The potassium abundance in the globular clusters
NGC 104, NGC 6752 and NGC 6809[*]

A. Mucciarelli[1,2], T. Merle[3], and M. Bellazzini[2]

[1] Dipartimento di Fisica e Astronomia, Università degli Studi di Bologna, Viale Berti Pichat, 6/2, 40127 Bologna, Italy
e-mail: `alessio.mucciarelli2@unibo.it`
[2] INAF–Osservatorio Astronomico di Bologna, via Ranzani 1, 40127 Bologna, Italy
[3] Institut d'Astronomie et d'Astrophysique, Université Libre de Bruxelles, CP.226, Boulevard du Triomphe, 1050 Brussels, Belgium

ABSTRACT

We derived potassium abundances in red-giant-branch stars in the Galactic globular clusters NGC 104 (144 stars), NGC 6752 (134 stars), and NGC 6809 (151 stars) using high-resolution spectra collected with FLAMES at the ESO – Very Large Telescope. In the samples we consider, we do not find significant intrinsic spreads in [K/Fe], which confirms the previous findings, but which is at variance with the cases of the massive clusters NGC 2419 and NGC 2808. Additionally, marginally significant [K/Fe]−[O/Fe] anti-correlations are found in NGC 104 and NGC 6809, and [K/Fe]−[Na/Fe] correlations are found in NGC 104 and NGC 6752. No evidence of [K/Fe]−[Mg/Fe] anti-correlation are found. The results of our analysis are consistent with a scenario in which the process leading to the multi-populations in globular clusters also implies enrichment in the K abundance, the amplitude of the associated [K/Fe] enhancement becoming measurable only in stars showing the most extreme effects of O and Mg depletion. Stars enhanced in [K/Fe] have so far only been found in clusters harbouring some Mg-poor stars, while the other globulars, without a Mg-poor sub-population, show small or null [K/Fe] spreads.

Key words. techniques: spectroscopic – globular clusters: individual: NGC 104 – globular clusters: individual: NGC 6752 – globular clusters: individual: NGC 6809 – stars: abundances

1. Introduction

The last decade of photometric and spectroscopic observations has significantly changed our view of the globular clusters (GCs). Considered for a long time as the simplest stellar populations available in the Universe, with all stars sharing the same age and chemical composition, GCs have revealed large and correlated star-to-star inhomogeneities in the abundance of several light elements, like C, N, Na, O, Mg, Al, and He (see, e.g., Gratton et al. 2012, for a thorough review). These inhomogeneities have been traced both in Galactic (Carretta et al. 2009a,b) and extragalactic GCs (Mucciarelli et al. 2009; Larsen et al. 2014). Their effects are also observed and recognized in the color magnitude diagrams of GCs, once the right combination of colours is adopted (see, e.g., Piotto et al. 2015; Milone et al. 2012; Lardo et al. 2011, and references therein). The photometric evidence, in particular, strongly suggests the presence of multiple discrete stellar populations in GCs (see e.g., Milone et al. 2015).

These chemical anomalies are usually interpreted as being due to self-enrichment of a gas polluted by the proton capture processes (the high temperature extension of the CNO-cycle) that is ejected at a sufficiently low velocity to be retained in the shallow potential well of proto-GCs. The candidate polluters that have been more exhaustively considered in the literature are intermediate-mass asymptotic giant branch (AGB) stars (D'Antona et al. 2002, 2005), fast rotating

massive stars (Decressin et al. 2007), interacting massive binary stars (De Mink et al. 2009), and/or super-massive stars (Denissenkov & Hartwick 2014; Denissenkov et al. 2015).

The precise identification of the polluter stars, the timescale of the self-enrichment process, and the actual process leading to the observed present-day status of GCs are widely debated and we still lack a convincing comprehensive model (see, e.g., Decressin et al. 2007; D'Ercole et al. 2008; De Mink et al. 2009; Bastian et al. 2013; Trenti et al. 2015). As noted, it is far from straightforward to reconcile the overall observational scenario with a unique self-enrichment process (Bastian et al. 2015).

Recently, potassium has joined the exclusive club of chemical elements involved in the chemical anomalies in GCs. The first evidence of an intrinsic spread in the K abundance has been provided for the massive and remote GC NGC 2419. Mucciarelli et al. (2012) analysed a sample of 49 giant stars by using DEIMOS@Keck low-resolution spectra and finding a huge distribution of the [K/Fe] abundance ratio, ranging from solar values up to +2.0 dex. Additionally, NGC 2419 shows a large anti-correlation between [K/Fe] and [Mg/Fe], which also spans an unusually large (∼2 dex) range of abundances. These results were confirmed by a high-resolution spectroscopy study of 13 red-giant-branch (RGB) stars by Cohen & Kirby (2012).

Further evidence of an intrinsic spread in the K abundances has been provided by Mucciarelli et al. (2015) for the massive cluster NGC 2808, one of the few Galactic GCs hosting stars with sub-solar [Mg/Fe] abundances, similar to those observed in NGC 2419. The intrinsic [K/Fe] spread detected in NGC 2808 is significant, but its amplitude is much smaller than that found in NGC 2419 (∼0.3 dex vs. ∼2.0 dex). Also, [K/Fe] abundance

---

ratios show significant correlations with [Na/Fe] and [Al/Fe], and anti-correlations with [O/Fe] and [Mg/Fe]. In particular, all the stars in NGC 2808 with [Mg/Fe] < 0.0 dex (hereafter Mg-deficient stars) show K abundances higher than those measured in stars with normal Mg abundances, fully analogous to the case of NGC 2419. On this basis, Mucciarelli et al. (2015) conclude that the [K/Fe] enhancement detected in the Mg-poor stars of these two clusters and the K-Mg anti-correlations are ascribable to the same self-enrichment process responsible of the observed chemical anomalies.

Carretta et al. (2013) measured the K abundance in a handful of stars in each of seven GCs (namely, NGC 6752, NGC 6121, NGC 1904, ω Centauri, 47 Tucanae, NGC 7099, and NGC 6397). They did not find any evidence of intrinsic K spread in these clusters. Moreover, the mean [K/Fe] and [Fe/H] ratios of the considered clusters appear to lie onto the same [K/Fe] vs. [Fe/H] relation defined by field stars. However we emphasize that none of the stars studied by Carretta et al. (2013) has [Mg/Fe] < 0.0. Hence they have not probed the extreme Mg-deficient population that is the main driver of the [K/Fe] vs. [Mg/Fe] anti-correlation in NGC 2419 and NGC 2808. We point out that the overall scenario of K abundances in Galactic field stars is not well understood, both from the observational and theoretical point of view (Romano et al. 2010).

Up until now, the only available theoretical study on the K abundance in GCs has been performed within the framework of AGB-driven self-enrichment, with the specific aim of reproducing the Mg-K anti-correlation observed in NGC 2419 (Ventura et al. 2012). In this basic model, super-AGB stars, that ignite the carbon burning in conditions of partial degeneracy until the formation of an O-Ne core, produce fresh potassium by proton captures on Argon nuclei, qualitatively reproducing the observations of NGC 2419 under certain assumptions, in particular on the highly uncertain cross section of the ^{38}Ar$(p, \gamma)^{39}$K reaction. A similar conclusion was reached by Iliadis et al. (2016) who investigate the temperature-density conditions that are able to reproduce the chemical anomalies observed in NGC 2419: they rule out that low-mass, AGB and massive stars can account for the observed chemical patterns, while super-AGB stars could be promising polluter stars (but the stellar model parameters need to be fine-tuned to produce the required temperatures).

In this paper, within an observational programme aimed at exploring the role of potassium in the process of self-enrichment of GCs, we investigate the K abundance and its relations with the light elements involved in the multiple populations in three GCs, namely NGC 104, NGC 6752, and NGC 6809.

2. Clusters selection

The three target clusters have been selected according to the following criteria:

1. GCs already analyzed by Carretta et al. (2009a,b), i.e., targeting stars whose membership have been already established and whose atmospheric parameters, metallicity, and light-elements abundances have been already accurately and homogeneously estimated;
2. GCs covering a wide metallicity range: we selected a metal-rich GC (NGC 104, [Fe/H] = –0.76 dex), a metal-intermediate GC (NGC 6752, [Fe/H] = –1.55 dex), and a metal-poor cluster (NGC 6809, [Fe/H] = –1.93 dex), according to the metallicity scale provided by Carretta et al. (2009c);

3. GCs with wide and clear Na-O anti-correlations, signature of a high efficiency of the self-enrichment process, albeit less extreme than in NGC 2808 and NGC 2419;
4. GCs close enough to provide relatively bright (V < 15.5) RGB stars as unchallenging spectroscopic targets.

3. Observations

Spectroscopic observations have been secured with the multi-object spectrograph FLAMES (Pasquini et al. 2000) mounted at the Very Large Telescope of the European Southern Observatory. We used FLAMES in the UVES+GIRAFFE combined mode, which enables the simultaneous allocation of 132 GIRAFFE-MEDUSA mid-resolution fibers and eight UVES high-resolution fibers over a field of view of ~25 arcmin diameter. The employed instrumental configurations are the HR18 GIRAFFE setup, covering from 7648 to 7889 Å and with a spectral resolution of 18 400, and the Red Arm CD#4 860 UVES setup, with a spectral coverage of 6600–10 600 Å and a spectral resolution of 47 000. The adopted UVES and GIRAFFE setups have been chosen because they sample the K I resonance line at 7699 Å.

To have a complete set of K, O, Na, Mg, and Al abundances for the cluster stars, we re-observed the same stars already observed by Carretta et al. (2007, 2009a,b) in their spectroscopic survey devoted to study Na and O abundances in GCs (hereafter, we refer to this spectroscopic survey as CAR). We refer to these papers for the description of the targets selection. Owing to some FLAMES fibers currently broken or parked, a few stars previously observed cannot be duplicated in our observations. For each cluster, two target configurations have been observed to guarantee the maximum overlap with the previous observations. Two observations of 1330 s each were secured for each target configuration.

Spectral reduction has been performed with the dedicated ESO pipelines[1], including bias subtraction, flat-fielding, wavelength calibration with a reference Th-Ar lamp, extraction of the 1-dimensional spectra and (only for UVES spectra) merging of the overlapping orders.

In a few cases, where the K I line is damaged for the occurrence of a cosmic ray in one of the exposures, only the other spectrum was used. For all the other cases, the individual exposures have been coadded together, after which they were corrected for their proper heliocentric velocity. The final spectra have on average S/N per pixel of between ~60–70 for the faintest stars (V ~ 15.5) and up to ~400 for the brightest targets (V ~ 11.5).

We summarize the key information about the observations of the target clusters below. We note that we excluded from our analysis the stars identified by CAR as field stars according to their radial velocity or with uncertain/unreliable (V − K) colors, hence with uncertain atmospheric parameters.

1. *NGC 104* – a total of 145 giant stars have been observed with GIRAFFE, 11 of them have also been observed with UVES. Two stars of Carretta et al. (2009b) are not included in our sample, namely #24553 and #35454.
2. *NGC 6752* – a total of 135 stars were observed with GIRAFFE, seven of them also observed as UVES targets, while eight other stars were observed only with UVES. Only the star #19714 of Carretta et al. (2007) was not observed.

---

[1] http://www.eso.org/sci/software/pipelines/

3. *NGC 6809* – a total of 153 stars were observed with GIRAFFE. Three stars of the original sample of Carretta et al. (2009a; namely #7000296, #7000057, and #6000017) did not reply. Thirteen stars were taken with UVES and only one of them is not in common with the GIRAFFE sample.

4. Radial velocities

Radial velocities were measured with DAOSPEC (Stetson & Pancino 2008) using tens of metallic lines available in the considered spectral range. The accuracy of the wavelength calibration has been checked by measuring the position of the emission sky lines and comparing them with their rest-frame position listed in Osterbrock et al. (1996), finding no significant shift. Typical uncertainties in radial velocities, computed as the dispersion of the mean divided by the root mean squares of the number of lines, are ∼0.4–0.7 km s^{-1}. The measured radial velocities have been compared with those obtained by CAR, to identify possible binary stars. In the distribution of radial velocity differences between our measures and those by CAR (Δ_{RV}) as a function of V magnitude, we identified four >3σ outliers, which we classify as candidate binary systems: one star in NGC 104 (#22726), one star in NGC 6752 (#21828), and two stars in NGC 6809 (#7000106 and #7000492). These stars have been excluded from the following analysis. The observed differences in radial velocity between the two epochs (in the sense this study – CAR) for these stars are Δ_{RV} = −14.3 km s^{-1}, Δ_{RV} = −7.6 km s^{-1}, Δ_{RV} = +5.5 km s^{-1} and Δ_{RV} = +2.9 km s^{-1}, respectively, where the typical dispersion in Δ_{RV} is <1.0 km s^{-1}, nearly independent of the star magnitude.

The average differences between our measures and those by CAR are (excluding the candidate binary stars) +0.01 km s^{-1} (σ = 0.40 km s^{-1}) for NGC 104, –0.18 km s^{-1} (σ = 0.67 km s^{-1}) for NGC 6752 and –0.15 km s^{-1} (σ = 0.78 km s^{-1}) for NGC 6809. We note that the standard deviation increases as the cluster metallicity decreases, owing to the associate decrease in the number of spectral lines that can be used to estimate radial velocities.

5. Chemical analysis

The K abundances were derived with the code GALA (Mucciarelli et al. 2013), by matching the measured and theoretical equivalent widths (EWs) of the resonance K line at 7699 Å. Model atmospheres have been obtained by interpolating in the MARCS model grid with standard chemical composition (Gustafsson et al. 2008) and assuming an overall metallicity [M/H] that matches the average iron abundance of each cluster, as provided by Carretta et al. (2009c). The adopted oscillator strength for the K line at 7699 Å is log(gf) = –0.176 from the NIST database while, for the Van der Waals damping constant, we used the value quoted by Barklem et al. (2000), namely log γ_{VdW}/N_H = 7.445. The adopted solar abundance is $K_\odot$ = 5.11 (Caffau et al. 2011). The K abundances of the stars of a given cluster were rescaled adopting the average [Fe/H] abundance, as quoted by Carretta et al. (2009c).

EWs have been measured with the code DAOSPEC, launched automatically with the wrapper 4DAO (Mucciarelli 2013) that also enables a visual inspection of the best-fit profile for each individual line. DAOSPEC performs the line-profile fitting under the assumption of a Gaussian profile. As a sanity check, we remeasured under IRAF the EW of some strong K I lines with EW larger than ∼200 mÅ, assuming a Voigt profile. The difference in the measured EWs are negligible, of the order of 1 mÅ or less, confirming that the assumption of a Gaussian profile is adequate for the strongest K lines at the used spectral resolution.

Because the K line at 7699 Å is located on the red side of the telluric *A* band, we carefully checked in all the target stars whether the K line was blended with a telluric feature. According to their radial velocity, only some stars of NGC 6809 are marginally contaminated. To clean the K line, we used appropriate synthetic spectra of the atmospheric transmission calculated with the TAPAS tool (Bertaux et al. 2014), taking into account the specific observing conditions of our data.

As summarised above, a total of 18 stars were observed both with UVES and GIRAFFE fibers. To check the stability of the measured EWs with respect to the spectral resolution (in particular related to the continuum placement), we compared the EWs of the K line measured with UVES and GIRAFFE. An average difference of –0.02 ± 0.8 mÅ (σ = 4.5 mÅ) is found, ensuring that no systematic difference exist between the two sets of EWs.

Table 1 lists the adopted atmospheric parameters, the measured EWs, and the derived [K/Fe] abundance ratios and the corresponding uncertainties for each target star.

5.1. Atmospheric parameters

The adopted effective temperatures (T_{eff}) and surface gravities (log g) are those derived photometrically by CAR. The adoption of the microturbulent velocity (v_t) for these stars require special care. The K line is a saturated line (up to ∼250 mÅ for the brightest stars in NGC 104, the most metal-rich GC of the sample) located close or along the flat portion of the curve of growth; thus, the abundances derived from this transition can be very sensitive to the microturbulent velocity (at variance with the weaker lines located on the linear part of the curve of growth). Our first attempt is to use v_t derived by CAR by imposing no trend between the theoretical EWs and the abundance of the iron lines. Adopting these values, for all the clusters, we found a clear trend between the [K/Fe] abundance ratio and v_t (see left panels of Fig. 1), while no trend is found between [K/Fe] and T_{eff} and between [K/Fe] and log g. Also, we note that the slope between [K/Fe] and v_t is fully compatible with the variation of [K/Fe] owing to a change of this parameter (the effect on [K/Fe] of a change of v_t is shown as an arrow in the upper-left panel of Fig. 1). As explained by Carretta et al. (2014) concerning the v_t derived using weak lines, "the values of v_t obtained with this technique are unsuitable when applied to strong lines such as the Na D or the Ba lines, resulting in strong trends as a function of the microturbulent velocity". In fact, we checked that the EW of the K line is always stronger than that of the strongest Fe I lines used by CAR to infer v_t (E. Carretta, priv. comm.). All these evidence suggest that the v_t scale derived by CAR is not appropriate for a saturated line as the K line used in this work (but they remain appropriate for weaker transitions).

A similar result has been found by Worley et al. (2013) that determined Ba abundances for giant stars in the globular cluster M15, testing different assumptions of v_t (see their Fig. 3). Similar to the K line, also the Ba lines are strong and sensitive to v_t. Worley et al. (2013) find a trend between Ba abundances and v_t when the original v_t values inferred by CAR are adopted. The same approach was adopted by Carretta et al. (2014). In all three cluster targets the v_t by CAR span large ranges of values (more than 1 km s^{-1}, with the extreme case of NGC 6809, where the stars range from 0.21 to 2.29 km s^{-1}). Such wide ranges seems

Table 1. Atmospheric parameters (T_{eff}, $\log g$ and v_t), measured EWs of the K I line at 7699 Å, [K/Fe] abundance ratios and their uncertainties for all the target stars.

Cluster	ID	T_{eff} (K)	$\log g$	v_t (km s^{-1})	EW (mA)	[K/Fe]$_{NLTE}$ (dex)
NGC 104	1389	4568	2.09	1.65	184.50	−0.07 ± 0.09
NGC 104	2608	3991	0.99	1.90	247.10	−0.11 ± 0.10
NGC 104	2871	4609	2.17	1.63	174.80	−0.15 ± 0.08
NGC 104	4373	4709	2.38	1.58	174.90	−0.06 ± 0.08
NGC 104	5172	4560	2.08	1.65	183.30	−0.09 ± 0.09
NGC 104	5270	3999	1.01	1.90	246.50	−0.10 ± 0.10
NGC 104	5277	4237	1.48	1.79	219.50	−0.03 ± 0.10
NGC 104	5640	4752	2.47	1.56	171.40	−0.05 ± 0.06
NGC 104	6092	4627	2.21	1.62	182.60	−0.04 ± 0.08
NGC 104	6808	4577	2.11	1.64	193.10	+0.04 ± 0.08
NGC 104	7711	4649	2.25	1.61	186.00	+0.02 ± 0.08
NGC 104	7904	4637	2.23	1.62	168.70	−0.20 ± 0.08
NGC 104	9163	4418	1.81	1.71	198.40	−0.05 ± 0.09
NGC 104	9268	4752	2.47	1.56	166.40	−0.11 ± 0.08
NGC 104	9518	4463	1.90	1.69	194.70	−0.05 ± 0.09
NGC 104	9717	4585	2.13	1.64	178.90	−0.12 ± 0.09

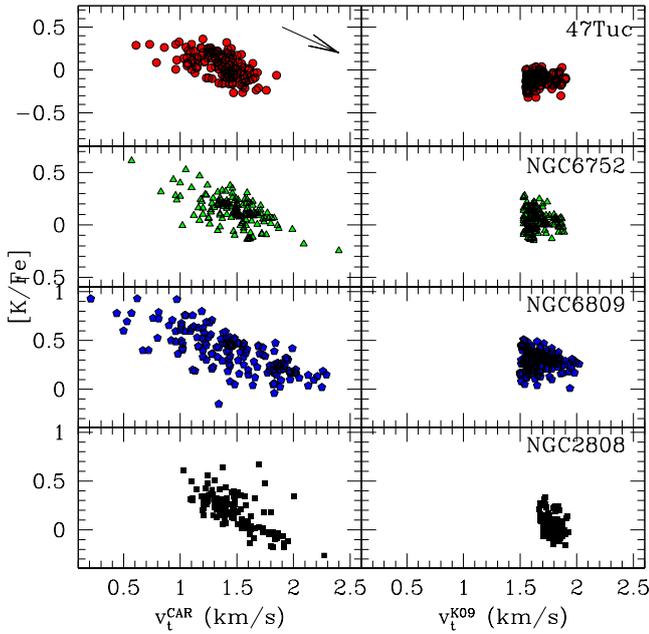**Notes.** The full table is available at the CDS.

Fig. 1. *Left panels*: behaviour of the [K/Fe] as a function of v_t provided by CAR. Red circles are the stars of NGC 104, green triangles those of NGC 6752, blue pentagons those of NGC 6809. *Right panels*: behaviour of the [K/Fe] as a function of v_t derived according to Kirby et al. (2009). The stars of NGC 2808 (black squares, Mucciarelli et al. 2015) are shown for comparison in the lowest panels. The arrow in the *upper-left panel* shows the effect on [K/Fe] of the change in v_t.

Fig. 2. Behaviour of the [K/Fe] as a function of T_{eff} (*left panels*), $\log g$ (*middle panels*), and v_t (*right panels*). Grey lines represent the linear fits.

remarkably unlikely, in particular with respect to the values of v_t obtained from high-resolution spectra, hence based on a large number of iron lines (see e.g. Carretta et al. 2009b). Also, our target stars cover a small region in the T_{eff}–$\log g$ space (only the brightest portion of the RGB), hence they are expected to cover a smaller range of v_t.

As per Mucciarelli et al. (2015), we adopt the relation by Kirby et al. (2009) that provides v_t as a function of $\log g$. This relation was obtained with a linear fit between $\log g$ and v_t (the latter derived spectroscopically) of a compilation of
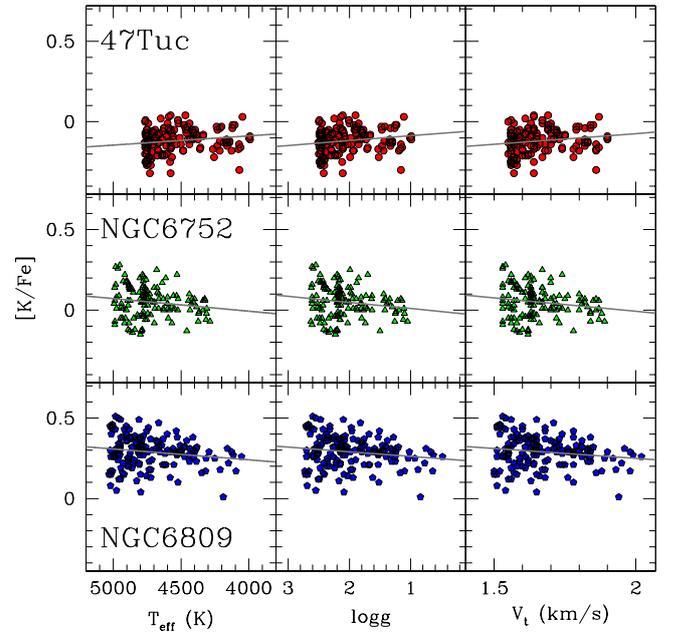
high-resolution measurements available in literature (see the references in Kirby et al. 2009). The v_t values obtained with this relation range from ~1.5 km s^{-1} to ~2 km s^{-1}; the cut at ~1.5 km s^{-1} visible in all the clusters reflects the similar luminosity (and gravity) limit reached by the faintest targets of the three GCs. The [K/Fe] abundance ratios derived with the Kirby et al. (2009) calibration do not exhibit peculiar or significant trend with T_{eff}, $\log g$ and v_t, as shown in Fig. 2.

5.2. Uncertainties

Two sources of uncertainties in the K abundance were taken into account, one arising from the EW measurement and one arising from the uncertainties in the adopted atmospheric parameters.

The uncertainty in the EW measurement of the K line was estimated by DAOSPEC according to the residual of the line fitting and then translated in abundance uncertainty. Owing to the high S/N of the spectra and the strength of the K line, the abundance uncertainties associated with the measurement errors range from ~0.01 to ~0.05 dex.

The K abundance derived from the line at 7699 Å is mainly sensitive to T_{eff} and v_t. We adopted the typical uncertainties in T_{eff} quoted by CAR (40 K for NGC 104, 58 K for NGC 6752, and NGC 6809): a change in T_{eff} of ±50 K changes the K abundance of about ±0.07 dex. The typical uncertainties in $\log g$ quoted by CAR (0.06 for all these three clusters) have a negligible impact (at a level of 0.01 dex) on the K abundance. On the other hand, this type of variation of $\log g$ leads to a change in v_t of ~0.01−0.02 km s^{-1}, according to the relation by Kirby et al. (2009). Considering this variation and the uncertainty of the relation by Kirby et al. (2009), we estimated a typical internal uncertainty in v_t of ±0.05 km s^{-1} that changes the K abundance of ∓0.03 dex. The total uncertainty for [K/Fe] is typically about 0.10−0.12 dex.

6. NLTE corrections

We consistently solved the statistical equilibrium and radiative transfer for populations and lines of the K I species using the NLTE radiative transfer code MULTI (version 2.3) (Carlsson 1986; Carlsson & Stein 1992). Since the K I species is like a trace element, the possible NLTE effects on the atmosphere was neglected as is usual. We use LTE model atmospheres from MARCS (Gustafsson et al. 2008). Continuous and line opacities for the other species are treated in LTE using the Uppsala package for the former as included in MULTI, and VALD atomic data for the latter. The K model atom has been computed with the automatic tool FORMATO (T. Merle et al., in prep.) For the purpose of the study, we only need to consider the fine structure of the first excited level of K to recover properly the resonant doublet. Energy levels from NIST were used and completed with levels 6g ^{2}G and 6h ^{2}H° from Park (1971) as done in Bruls et al. (1992). The radiative bound-bound transitions between the mean levels have been obtained from the combination of the individual lines from the VALD database. In addition, we add nine multiplets (doublets and triplets) from Bruls et al. (1992) not present in the VALD database and some of them using the added levels 6g ^{2}G and 6h ^{2}H°. For the 7699 Å line, we used the same atomic data used in the chemical analysis (see Sect. 5).

The bound-bound electron collision transitions were computed using the Van Regemorter formula (van Regemorter 1962), based on the oscillator strength of the corresponding radiative transitions. For collision transition without radiative counterpart, a default value for the effective collision strength is set to unity. The bound-free electron collisions were computed with the Seaton formula (Seaton 1962), using the radiative photoionization cross-section counterpart at the threshold.

The grid of NLTE correction for the K abundances from the 7699 Å line used in this study was calculated on the basis of the range of atmospheric parameters of the observed GCs. In particular, seven effective temperatures T_{eff} = 3900, 4000, 4250, 4500, 4750, 5000, 5250 K, six surface gravities $\log g$ = 0.5, 1.0, 1.5, 2.0, 2.5, 3.0 dex, three overall metallicities corresponding to the mean metallicity of the GCs, and two microturbulent velocities v_t = 1 and 2 km s^{-1}, were considered. For each metallicity, we also vary the K abundance by step of 0.3 dex, from [K/Fe] = −0.9 and +0.9 dex. For each target star, we calculated the corresponding NLTE abundance correction by interpolating into the

grid to find the NLTE K abundance that fits the corresponding observed equivalent width of the K I 7699 Å line.

The NLTE abundance corrections for this line ($\Delta A(\mathrm{K})$ = $A(\mathrm{K})_{\mathrm{NLTE}} − A(\mathrm{K})_{\mathrm{LTE}}$) depend strongly on the atmospheric parameters as shown in the first three panels of Fig. 3. The corrections are always negative, meaning that the K abundance is always overestimated in LTE owing to the scattering in this resonance line. For the range of the atmospheric parameters considered for the three GCs, the abundance corrections is between −0.54 and −0.03 dex. The correction increases with T_{eff} and $\log g$ and decreases with the K abundance. We estimate that the typical uncertainties in the atmospheric parameters quoted in Sect. 5.2 translate into variations of $\Delta A(\mathrm{K})$ of the order of ±0.02−0.03 dex.

The main sources of uncertainties in the calculation of NLTE corrections come from photoionizations and H collisions.

No quantum mechanical data exist for the photoionization of the energy levels of this element. The radiative bound-free transition of the ground stage come from a fit of experimental measurements. At the photoionisation threshold (2706.36 Å), Sandner et al. (1981) provides a cross-section of σ = 3.5 × 10−22 cm^{-2}. For the dependance of the cross-section away from threshold, we used the values from (Rahman-Attia et al. 1986) based on the quantum-defect method. For all other levels, we used hydrogenic approximation (Kramer's law) with a bound-free Gaunt factor depending on principal and secondary quantum numbers computed thanks to the formulation of Karzas & Latter (1961) implemented by Janicki (1990).

The sensitivity to the H collisions has also been investigated. Using the Drawin formula (Drawin 1969) with a scaling factor of 1, we recalculate a complete grid and re-estimate the complete NLTE abundance corrections. We show the comparison in the lower-right panel of Fig. 3 between these two sets of corrections. The NLTE abundance correction is slightly reduced when inelastic hydrogen collisions are included. The average K abundances vary by less than 0.05 dex and all the results discussed in the next section are not affected by this choice.

Nevertheless, we emphasise that the Drawin's formula does not have a correct physical background. It has recently been shown by Barklem et al. (2011) that the Drawin's formula compares poorly with the results of available full quantum scattering calculations based on detailed quantum mechanical studies. But in the absence of any quantum mechanical data for collisions between potassium and hydrogen, the Drawin's formula was used to estimate the possible uncertainties in the NLTE calculations.

7. Potassium abundances

7.1. Potassium abundance spread

The mean K abundance of each cluster was calculated with the maximum likelihood algorithm described in Mucciarelli et al. (2012), which also provides the intrinsic spread (σ_{int}) and the associated uncertainty, calculated by taking into account the uncertainties for each individual star. Table 2 lists the derived average abundance for each cluster, together with the value of the observed and intrinsic dispersion, the number of stars and the cluster metallicity.
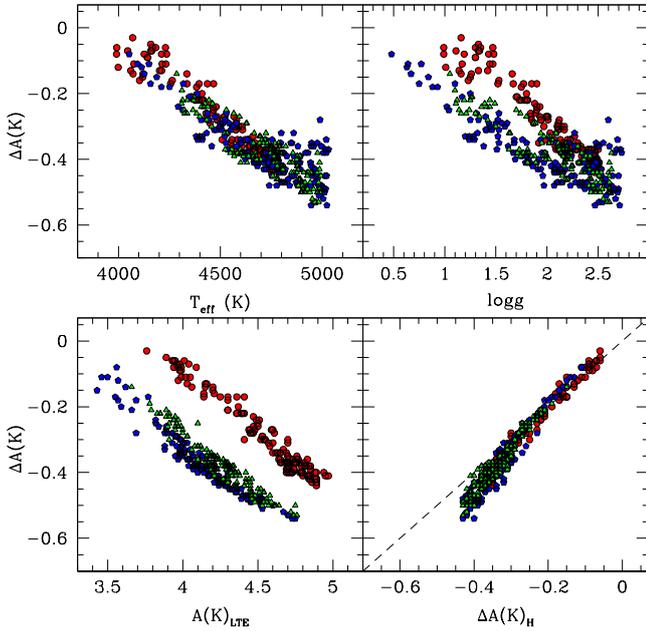
In the case of NGC 6809, the derived average abundance is ⟨[K/Fe]⟩ = +0.29 ± 0.01 dex with an observed scatter of σ_{obs} = 0.10 dex and an intrinsic scatter of σ_{int} = 0.02 ± 0.02 dex. NGC 6809 is not included in the sample analysed by Carretta et al. (2013) and no additional measures of K abundances are available in the literature.

Table 2. Average [K/Fe], observed (σ_{obs}) and intrinsic (σ_{int}), number of measured stars and average [Fe/H] for the three target GCs.

Cluster	$\langle[K/Fe]_{NLTE}\rangle$	σ_{obs}	σ_{int}	N_{stars}	$\langle[Fe/H]\rangle$
NGC 104	−0.12 ± 0.01	0.08	0.00 ± 0.02	144	−0.76
NGC 6752	+0.05 ± 0.01	0.10	0.02 ± 0.03	134	−1.55
NGC 6809	+0.29 ± 0.01	0.10	0.02 ± 0.02	151	−1.93

Table 3. Spearman correlation coefficient and associated two-tailed probability for the [K/Fe] abundance ratio against [O/Fe], [Na/Fe], [Mg/Fe], and [Al/Fe].

Cluster	[K/Fe]–[O/Fe]	[K/Fe]–[Na/Fe]	[K/Fe]−[Mg/Fe]	[K/Fe]−[Al/Fe]
NGC 104	$C_S = −0.27$	$C_S = +0.20$	$C_S = −0.30$	$C_S = +0.28$
	$P = 0.0035$	$P = 0.017$	$P = 0.37$	$P = 0.40$
NGC 6752	$C_S = −0.18$	$C_S = +0.24$	$C_S = −0.16$	$C_S = −0.06$
	$P = 0.068$	$P = 0.0065$	$P = 0.59$	$P = 0.84$
NGC 6809	$C_S = −0.20$	$C_S = +0.11$	$C_S = −0.37$	$C_S = +0.38$
	$P = 0.035$	$P = 0.22$	$P = 0.19$	$P = 0.19$

Fig. 3. Behaviour of the difference between NLTE and LTE potassium abundance (calculated without including H collisions) as a function of T_{eff} (*upper-left panel*), log g (*upper-right panel*) and $A(K)_{LTE}$ (*lower-left panel*). *Lower-right panel*: comparison between the NLTE correction calculated with and without the inclusion of H collisions. Same symbols used as Fig. 1.

Fig. 4. Behaviour of [K/Fe] as a function of [Na/Fe]. Same symbols as in Fig. 1. Black squares represent the comparison stars of NGC 2808 (Mucciarelli et al. 2015).

For NGC 6752 we derived an average abundance of $\langle[K/Fe]\rangle = +0.04 ± 0.01$ dex, with an observed dispersion $\sigma_{obs} = 0.10$ dex. Also for this cluster, the observed scatter is compatible with null intrinsic scatter, with $\sigma_{int} = 0.02 ± 0.03$ dex. Carretta et al. (2013) derive an abundance of $\langle[K/Fe]\rangle = +0.17 ± 0.04$ dex from 25 turnoff and RGB stars.

For NGC 104, we derived a mean abundance $\langle[K/Fe]\rangle = −0.12 ± 0.01$ dex, with an observed dispersion $\sigma_{obs} = 0.08$ dex that is fully compatible with a zero-scatter ($\sigma_{int} = 0.00 ± 0.02$ dex). The mean derived by Carretta et al. (2013) ($\langle[K/Fe]\rangle = +0.14 ± 0.03$) from the analysis of 12 turnoff and sub-giant stars (no star is in common with our sample) is formally incompatible with our value. However, we check that the differences with Carretta et al. (2013) for NGC 6752 and NGC 104 can be easily ascribed to differences in the adopted model atmospheres

(ATLAS9 vs. MARCS) and NLTE corrections (Takeda et al. 2002 vs. our own computations, see Sect. 6).

In conclusion, we confirm the results by Carretta et al. (2013), i.e., that these clusters do not display a measurable intrinsic scatter in the abundance of potassium. Also, in this case, we note that no Mg-deficient star is known in the GCs analysed here (Carretta et al. 2009b).

7.2. Potassium and light element abundances

Figures 4–7 show the behaviour of [K/Fe] as a function of [Na/Fe], [O/Fe], [Mg/Fe] and [Al/Fe] (as derived by CAR) for the three clusters considered here plus NGC 2808 (from Mucciarelli et al. 2015), taken as a reference case ([Fe/H] = −1.18 dex). For each pair [K/Fe]−[X/Fe] (with X indicating Na, O, Mg and Al) we calculated the non-parametric Spearman correlation coefficient (C_S) and the corresponding two-tailed
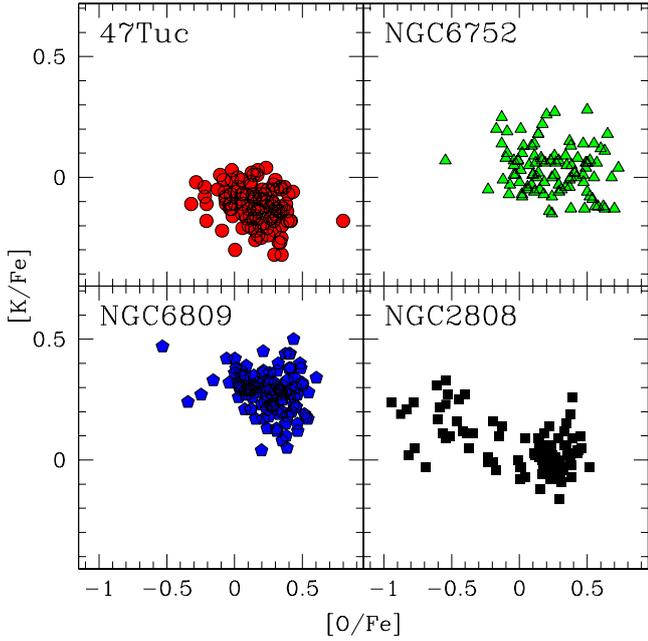
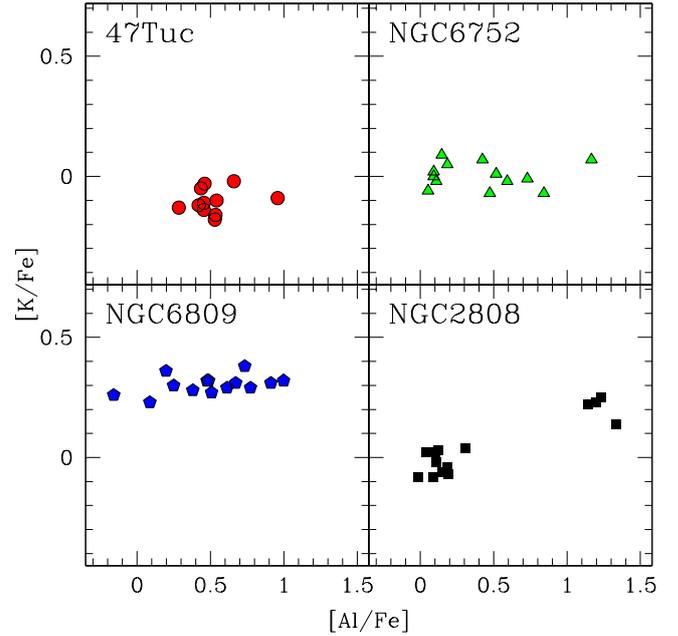**Fig. 5.** Behaviour of [K/Fe] as a function of [O/Fe] (same symbols as in Fig. 4).

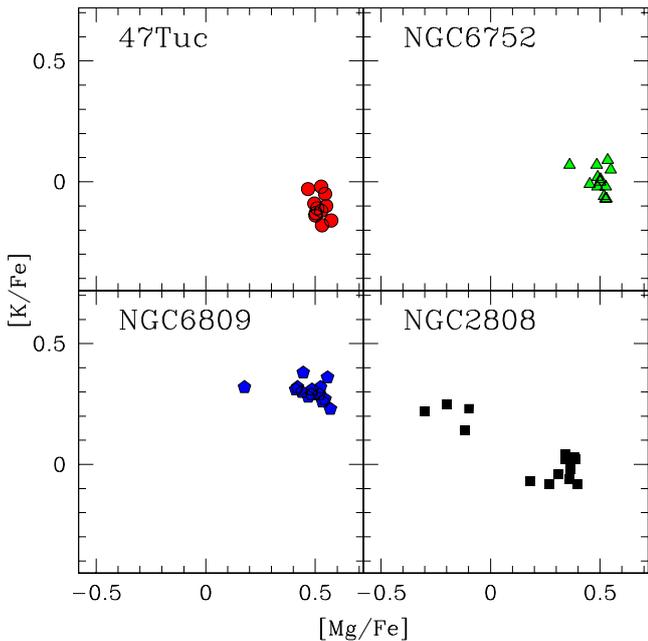**Fig. 7.** Behaviour of [K/Fe] as a function of [Al/Fe], only for the UVES targets (same symbols as in Fig. 4).

Fig. 6. Behaviour of [K/Fe] as a function of [Mg/Fe], only for the UVES targets (same symbols as in Fig. 4).

probability P that a C_S larger than (or equal to) the observed one (in absolute value) may arise from non-correlated random variables. The results are listed in Table 3.

Figures 4 and 5, where the large samples enable a deeper insight, deserve some comment. [K/Fe] is found to correlate with [Na/Fe] in NGC 6752 and NGC 104, while no correlation is found in NGC 6809. On the other hand, [K/Fe] is found to anti-correlate [O/Fe] in NGC 104, while the other two clusters show weak hints of anti-correlation. The behaviour is very similar to that observed in NGC 2808, with smaller amplitudes, and, in some cases, the correlation seems marginally significant. In particular, the probability that the C_S observed for the [K/Fe] vs.

[O/Fe] correlation in NGC 104 occurred by chance is as low as 0.35 per cent.

We checked whether the error distribution of the atmospheric parameter with the largest impact on the abundance estimates ($T_{\rm eff}$) can introduce spurious correlations between the considered abundance ratios via its known correlation with other parameters. An increase of $T_{\rm eff}$ corresponds to an increase of $\log g$ and a decrease of $v_{\rm t}$. These correlated changes of the atmospheric parameters lead to an increase of all the abundance ratios that we consider in this work. Thus, the uncertainties in the parameters could mimic a positive [K/Fe]−[Na/Fe] correlation but they are not able to introduce a [K/Fe]−[O/Fe] anti-correlation.

We remark that the Spearman correlation coefficient does not take into account the internal uncertainties in the individual abundance, at variance with the estimate of the intrinsic spread. This may suggest a possible overestimate of the internal uncertainties on individual [K/Fe] measures, which can hide small but real intrinsic spreads. For instance, if we decrease the internal uncertainty in $v_{\rm t}$ by a factor of 2, and repeat the maximum likelihood analysis, a non-null [K/Fe] spread of $0.04{-}0.05$ dex is found in all three clusters. On the other hand, we note that a similar change in the internal uncertainty in $v_{\rm t}$ also increases the internal spread detected in NGC 2808 by about a factor of 2. Hence, even if a real intrinsic spread in K abundance is present in NGC 104, NGC 6752, or NGC 6809, it is significantly smaller than that detected in NGC 2808. On the other hand, we must be aware that such very weak (but significant) correlations between abundance ratios can also be produced by small systematics errors in the atmospheric parameters or by subtle inadequacies of the model atmosphere, displaying an effect smaller than the uncertainty on the individual abundance estimate.

In the cases of Mg and Al, where a lower number of stars with simultaneous measures of K is available (Figs. 6 and 7) no obvious correlation is found. However, we note that, in the three GCs considered here, [K/Fe] and [Mg/Fe] exhibit the same behaviour with respect to [Al/Fe], i.e., they are virtually constant while [Al/Fe] spans about one full dex, while stars in NGC 2808 show a weak but significant positive correlation.

8. Conclusions

The main results of the K abundance analysis from high-resolution spectra in NGC 104, NGC 6752, and NGC 6809 can be summarised as follows:

(i) At variance with NGC 2419 and NGC 2808, where significant intrinsic star-to-star differences in the [K/Fe] abundance ratio have been detected, all three GCs discussed here are formally compatible with a null [K/Fe] spread, which is in agreement with previous findings by Carretta et al. (2013), based on smaller samples.

(ii) No hint of correlation between [K/Fe] and [Mg/Fe] or [Al/Fe] is found in NGC 104, NGC 6752, and NGC 6809; in particular none of them shows the [K/Fe]−[Mg/Fe] anti-correlation detected in NGC 2808 and NGC 2419. However the samples considered for these correlations are small and there is no known Mg-deficient star in the considered clusters.

(iii) [K/Fe] is found to correlate with [Na/Fe] and to anti-correlate to [O/Fe], possibly hinting at the presence of a real, albeit very small, intrinsic spread in K abundances, which may go undetected if the internal uncertainties are slightly overestimated. If this were the case, the spread should be significantly smaller than that measured in NGC 2808, typically ≤0.05 dex. If these correlations reflect real physics relations (and not, e.g., a slight inadequacy of the measuring procedure), they provide further support to the hypothesis that potassium also has a role in the multi-populations phenomenon.

All the evidence collected so far about K abundances in GCs, when considered within a self-enrichment scenario, suggests that K is an element produced within the same thermonuclear chains responsible of the enrichment/depletion of O, Na, Al, Mg etc. However, the magnitude of the [K/Fe] spread, as well as the correlations with other abundance ratios, varies from cluster to cluster, emerging beyond our sensitivity limit only in clusters where the process of GC self-enrichment reached the most extreme effects (Carretta 2014; Mucciarelli et al. 2015). At this stage this can be considered merely as a sound working hypothesis. The survey of K abundances must be extended, with particular attention to stars belonging to extreme second-generation stars (as defined in Carretta 2014), to get the observational basis sufficient to draw firmer conclusions.

References

Barklem, P. S., Piskunov, N., & O'Mara, B. J. 2000, A&AS, 142, 467
Barklem, P. S., Belyaev, A. K., Guitou, M., et al. 2011, A&A, 530, A94
Bastian, N., Lamers, H. J. G. L. M., de Mink, S. E., et al. 2013, MNRAS, 436, 2398
Bastian, N., Cabrera-Ziri, I., & Salaris, M. 2015, MNRAS, 449, 3333
Bertaux, J. L., Lallement, R., Ferron, S., Boonne, C., & Bodichon, R., 2014, A&A, 564, A46
Bruls, J. H. M. J., Rutten, R. J., & Shchukina, N. G. 1992, A&A, 265, 237
Caffau, E., Ludwig, H.-G., Steffen, M., Freytag, B., & Bonifacio, P. 2011, Solar Physics, 268, 255
Carlsson, M. 1986, Uppsala Astron. Obs. Rep., 33
Carlsson, M., & Stein, R. 1992, ASP Conf. Ser., 26, 515
Carretta, E. 2014, ApJ, 795, L28
Carretta, E., Bragaglia, A., Gratton, R. G., Lucatello, S., & Momany, Y. 2007, A&A, 464, 927
Carretta, E., Bragaglia, A., Gratton, R. G., et al. 2009a, A&A, 505, 117
Carretta, E., Bragaglia, A., Gratton, R. G., & Lucatello, S. 2009b, A&A, 505, 139
Carretta, E., Bragaglia, A., Gratton, R., D'Orazi, V., & Lucatello, S. 2009c, A&A, 508, 695
Carretta, E., Gratton, R. G., Bragaglia, A., et al. 2013, ApJ, 769, 40
Carretta, E., Bragaglia, A., Gratton, R. G., et al. 2014, A&A, 561, A87
Cohen, J. G., & Kirby, E. N. 2012, ApJ, 760, 86
D'Antona, F., Caloi, V., Montalbàn, J., Ventura, P., & Gratton, R. 2002, A&A, 395, 69
D'Antona, F., Bellazzini, M., Caloi, V., et al. 2005, ApJ, 631, 868
Decressin, T., Meynet, G., Charbonell, C., Prantzos, N., & Ekstrom, S. 2007, A&A, 464, 1029
De Mink, S. E., Pols, O. R., Langer, N., & Izzard, R. G. 2009, A&A, 507, L1
Denissonkov, P. A., & Hartwick, F. D. A. 2014, MNRAS, 437, 21
Denissonkov, P. A., VandenBerg, D. A., Hartwick, F. D. A., et al. 2015, MNRAS, 448, 3314
D'Ercole, A., Vesperini, E., D'Antona, F., McMillan, S. L. W., & Recchi, S. 2008, MNRAS, 391, 825
Drawin, H. W. 1969, Z. Phys., 225, 483
Gratton, R. G., Carretta, E., & Bragaglia, A. 2012, A&ARv, 20, 50
Gustafsson, B., Edvardsson, B., Eriksson, K., et al. 2008, A&A, 486, 951
Iliadis, C., Karakas, A. I., Prantzos, N., Lattanzio, J. C., & Doherty, C. L. 2016, ApJ, 818, 98
Janicki, C. 1990, Comput. Phys. Commun., 60, 281
Karzas, W. J., & Latter, R. 1961, ApJS, 6, 167
Kirby, E. N., Guhathakurta, P., Bolte, M., Sneden, C., & Geha, M. 2009, ApJ, 705, 328
Lardo, C., Bellazzini, M., Pancino, E., et al. 2011, A&A, 525, A114
Larsen, S. S., Brodie, J. P., Grundahl, F., & Strader, J. 2014, ApJ, 797, 15
Milone, A. P., Piotto, G., Bedin, L. R., et al. 2012, ApJ, 744, 58
Milone, A. P., Marino, A. F., Piotto, G., et al. 2015, ApJ, 808, 51
Mucciarelli, A. 2013, ArXiv e-prints [arXiv:1311.1403]
Mucciarelli, A., Origlia, L., Ferraro, F. R., & Pancino, E. 2009, ApJ, 695, L134
Mucciarelli, A., Bellazzini, M., Ibata, R., et al. 2012, MNRAS, 426, 2889
Mucciarelli, A., Pancino, E., Lovisi, L., Ferraro, F. R., & Lapenna, E. 2013, ApJ, 766, 78
Mucciarelli, A., Bellazzini, M., Merle, T., et al. 2015, ApJ, 801, 68
Osterbrock, D. E., Fulbright, J. P., Martel, A. R., et al. 1996, PASP, 108, 277
Park, C. 1971, J. Quant. Spectr. Rad. Transf., 11, 7
Pasquini, L., Avila, G., Allaert, E., et al. 2000, Proc. SPIE, 4008, 129
Piotto , G., Milone, A. P., Bedin, L. R., et al. 2015, AJ, 149, 91
Rahman-Attia, M., Jaouen, M., Laplance, G., & Rachman, A. 1986, J. Phys. B: At. Mol. Opt. Phys., 19, 897
Romano, D., Karakas, A. I., Tosi, M., & Matteucci, F. 2010, A&A, 522, A32
Sandner, W., Gallagher, T. F., Safinya, K. A., & Gounand, F. 1981, Phys. Rev. A, 23, 2732
Seaton, M. J. 1962, in Atomic and Molecular Processes (New York: Academic), ed. D. R. Bates, 375
Stetson, P., & Pancino, E., 2008, PASP, 120, 1332
Takeda, Y., Okhubo, M., & Sadakane, K. 2002, PASJ, 54, 451
Trenti, M., Padoan, P., & Jimenez, R. 2015, ApJ, 808, L35
van Regemorter, H. 1962, ApJ, 136, 906
Ventura, P., D'Antona, F., Di Criscienzo, M., et al. 2012, ApJ, 761, L30
Worley, C. C., Hill, V., Sobeck, J., & Carretta, E. 2013, A&A, 553, A47